Rev.Adv.Mater.Sci. 11 (2006) 56-78

OPTICAL AND ELECTRONIC PROPERTIES OF SMALL SIZE SEMICONDUCTOR NANOCRYSTALS AND NANOCLUSTERS*

Aristides D. Zdetsis

Department of Physics, University of Patras, 26500 Patras, Greece

Received: June 17, 2005

Abstract. Optical and electronic properties of small Si nanocrystals and selected nanoclusters are examined and critically reviewed within the framework of high level and high accuracy *ab initio* calculations based on 'static' and time-dependent density functional theory, using a hybrid nonlocal exchange and correlation functional. These calculations are supported by sophisticated quadratic configuration interaction and other multi-reference methods, such as multi-reference second order perturbation theory. Similar calculations for Ge and SiGe nanocrystals examine the origin of the gap, the role of surface oxygen or hydrogen and the critical dimensions for visible photoluminescence. The agreement of our theoretical predictions with accurate experimental results is excellent, despite other conflicting experimental and theoretical results. The main sources of conflict in the experimental results are oxygen contamination, preparation conditions and difficulties in size determination. The theoretical controversies are due to either poor treatment of correlation and exchange, or incorrect fitting of empirical parameters. In most of the conflicting studies agreement with experiment or theory is claimed. We illustrate, using as an additional example the Si_6 nanocluster, how easily a seemingly good agreement between theoretical and experimental results could be fortuitous and misleading. The results presented here are very promising for future extensions to the accurate study of nanowires and nanoropes as well as for band-gap engineering.

* Presented at the 2nd International Conference "Nanomaterials and Nanotechnologies" (Crete, Greece, June 14-18, 2005)

1. INTRODUCTION

The field of atomic nanoclusters (free or supported on substrates) and nanocrystals, which form a link between molecules and crystals, is very active over many years due to its fundamental scientific and technological importance, as a result of the novel properties of these nanosystems found neither in molecules nor in infinite solids. Contrary to nanoclusters, the nanocrystals preserve most of the symmetry properties of the corresponding infinite crystals, of which many times are used as model systems, although nowadays they can be readily produced by different technological techniques. Among the various types of atomic nanoclusters and nanocrystals the semiconductor nanocrystals (and nanoclusters) have a special technological importance especially for micro and nano-electronics. The optical properties of silicon nanocrystals, which are inherently connected with the electronic properties, have been a very challenging and promising field of research over the last decade for obvious technological and scientific reasons [1-31]. More recently some sporadic efforts have been extended over other 'silicon-like' (e.g. Ge) [32-37] and silicon based (e.g. SiGe) [38-40] nanocrystals. The main reason is that, contrary to the electronic, the optical properties of the corresponding bulk crystals (for instance Si and

Corresponding author: Aristides D. Zdetsis, e-mail: zdetsis@upatras.gr

Ge) are rather poor because of the small band gap and the resulting indirect phonon-assisted light emission. The culmination of the semiconductor nanocrystals research occurred with the observation of visible photoluminescence (PL) in porous silicon and silicon nanocrystals [1-14]. A large number of experimental and theoretical approaches have been carried out in order to explore the properties and resolve the origins of the observed visible photoluminescence [1-31], which was attributed to quantum confinement. However, even today there are still issues, which are considered by several researchers as unsettled. A major point of dispute, besides the origin of PL, is the variation of the optical gap as a function the nanocrystal size. For instance, the majority of the earlier experimental (and theoretical) work gives diverse results as for the size of the Si nanoparticles capable of emitting in the visible. The results of Wolkin *et al.* [3] revealed optical gaps as small as 2.2 eV, for nanoclusters with a diameter of 18 Å. For nanoclusters of about the same size Wilcoxon *et al.* [2] obtained a similar result (2.5 eV) together with a much larger gap of about 3.2 eV for highly purified samples of the same diameter. On the other hand, Schupler *et al.* [5] have estimated the critical diameter for visible PL to be less than 15 Å. As it will be demonstrated, most of the existing discrepancies in the experimental results are due to either oxygen contamination (or more generally to the preparation conditions), or experimental uncertainties in the determination of the nanocrystal diameter. The discrepancies in the *ab initio* theoretical calculations, especially in the region of diameters between 1 and 2 nm, are due to poor treatment of exchange and (to a lesser degree) of correlation, according to our well tested results [7]. Another source of error in phenomenological calculations (i.e empirical and semi-empirical approaches with adjustable parameters) for small-size nanocrystals is the choice of fitting key parameters of the method to bulk values. This could lead to relatively large errors for such small sizes of nanocrystals, due to the effects of quantum confinement. For the oxygen 'contaminated' nanocrystals, as will be shown below, the role of bonding environment and the possible surface reconstruction are also controversial issues. Recent studies about the role of surface oxygen on the optical properties of silicon nanoclusters report conflicting levels of importance, ranging from minimal to crucial. In many experiments, the presence of oxygen is considered as a means to effectively passivate the surface dangling bonds or as a means to reduce (through oxidation) the size of the silicon nanoparticles. In most of the cases oxygen is just a contaminant, which is very difficult to remove. In most of the realistic calculations the role of surface oxygen, has been ignored or underestimated, despite the evidence given by experiments [2, 3, 5, 10, 11, 14]. In the last two years, some high level model calculations for oxygenated nanocrystals have appeared [17, 18, 27, 29-31]. However, calculations on Ge ('Si-like') [32-37] and SiGe (Si-based) [38-40] nanocrystals are still very limited in number. The same is true for the corresponding experimental results. Controversial issues about the dependence of the optical gap of Ge nanocrystals versus their diameter exist here too for the same reasons as in Si nanocrystals. Contrary to Ge and SiGe nanocrystals where the literature is very limited, the literature for small silicon (nano)clusters, is extremely rich and the number of publications ranges to several hundredths or even thousandths [41-46]. Nevertheless here too, controversial results and interpretations do exist despite the widespread believe that most of the major problems are well understood and resolved, especially for the small clusters [46]. Surprisingly enough, even Si_6, which is considered as one of the best understood and extensively studied clusters, is full of puzzles and paradoxes about its molecular, electronic and optical structure [46]. In the present critical review we concentrate mainly on semiconductor nanocrystals, such as Si, Ge and SiGe nanocrystals with a special emphasis on their optical properties and in particular the optical absorption and emission of visible PL. This topic has particular importance for technological applications, especially in view of the mediocre optical performance of the corresponding infinite size (bulk) crystals. The central reference point of the present review is concentrated on the high-level high-accuracy calculations performed at the University of Patras by the present author and collaborators [7, 30, 31, 37, 39, 46]. These calculations have been performed within the framework of multi-referenced second order many-body perturbation theory (MR-MP2) [7, 30] and time-dependent density functional theory (TDDFT) [47], employing the hybrid nonlocal exchange-correlation functional of Becke, Lee, Yang and Parr (B3LYP) [48]. In several cases the non-hybrid functional of Becke and Perdew BP86 [49] has been used for comparison. The accuracy of the optical gap obtained by MR-MP2 or TTDFT/B3LYP is better than 0.3 eV. This type of accuracy allows safe conclusions about the origin and the magnitude of the gap (and the resulting visible PL) to be made, as well as for fair comparisons with other theoretical and experimental results. The B3LYP

functional, which can efficiently reproduce the band structure of crystalline Si, without the need for ad hoc numerical adjustments [50], is absolutely essential for this type of accuracy. Without overlooking the possibility that the present description could be considered as biased, it will be illustrated that this work can resolve (it has resolved already) many existing controversies and can bridge several conflicting views in the literature. The key point to achieve this is the confidence in a truly accurate method and the understanding of the misconception as to what the 'agreement' of theory with experiment or of theory with theory or even experiment with experiment really means. Usually the real and the idealized system are different. Sometimes, however, there is interesting physics underlying the discrepancies. To illustrate this point further, the additional example of Si_6 cluster has been selected for review. The present work is organized as follows: After an overview of the various theoretical approaches used in the literature in Section 2, an outlined of the present calculations is given in Section 3. In Section 4, both the pure hydrogen-passivated silicon nanocrystals (Si:H) as well as nanocrystals containing oxygen (Si:H,O) are discussed extensively. The exact role of oxygen for the optical properties of silicon nanocrystals and porous silicon, in conjunction with hydrogen and surface reconstruction, is described at more length in this section. In sections 5 the optical properties of Ge:H and SiGe:H nanocrystals are discussed relatively briefly and the possibilities of band-gap engineering through substitution (of Si with Ge) and doping are examined and explained. In section 6 the Si_6 cluster is briefly considered and discussed as a representative example of the inherent difficulties in the study of silicon clusters. In this section we will discus the interesting story of Si_6, leaving aside the more complete summary and discussion of Si nanoclusters for a future time. Finally, in the closing section 7, a few brief concluding remarks about some controversial issues are given, as an epilogue.

2. OVERVIEW OF THE THEORETICAL TECHNIQUES

The semiconductor nanocrystals in the range of sizes suitable for optoelectronic and other applications are usually too small to be described by k-space theoretical techniques, used for large size crystals. At the same time they are too big to be described by real-space high level *ab initio* quantum chemistry techniques, used for small molecules. Therefore both of these two categories of theoretical approaches, the 'atomistic' (real space) and the 'crystalline' (k-space), require special attention with specific strategies and further modifications or approximations in order to be applicable to 'small nanocrystals', which with atomistic standards are already much too large. For instance, a small Si nanocrystal with diameter about 2.5 nm consists of 281 Si atoms and 172 H atoms at the surface and includes 4,106 electrons. This is a huge many-body (many-electron) system, for which the time-independent Schrödinger equation in atomic units and obvious notation (here N=4,106, usually N=10^{23}) looks like:

$$\left\{-\frac{1}{2}\sum_{i=1}^{N}\nabla_i^2+\sum_{i=1}^{N}\upsilon(\mathbf{r}_i)+\frac{1}{2}\sum_{i=1}^{N}\sum_{\substack{i=1\\(j\neq 1)}}^{N}-\frac{1}{|\mathbf{r}_i-\mathbf{r}_j|}\right\} \cdot\Psi(\mathbf{r}_1,\mathbf{r}_2,\ldots\mathbf{r}_N)=E\Psi(\mathbf{r}_1,\mathbf{r}_2,\ldots\mathbf{r}_N). \quad (1)$$

The solution of this (system of) differential equation(s) is a formidable task. The main difficulty is the presence of the interaction term $\frac{1}{2}\sum_{i=1}^{N}\sum_{\substack{i=1\\(j\neq 1)}}^{N}-\frac{1}{|\mathbf{r}_i-\mathbf{r}_j|}$, which couples the coordinates of the *i*-th and *j*-th electron. The traditional *ab initio* approach to this many-body problem is based on the 'one-electron approximation'. Instead of considering all the electrons together, according to the one electron (one-body) approximation we look at the electrons one by one, replacing the complicating fluctuating forces due to the others by an average force known as a 'mean field'. This trick reduces the 4,106 coupled three dimensional differential Schrödinger's equations to one much simpler three-dimensional equation for each electron (which, obviously, must be solved only once). However, the mean field depends on the electron density, which is not known until the one-electron problem has been solved to find all the one-electron quantum states. Therefore it is necessary to use some sort of iterative procedure to form a consistent solution. The traditional *ab initio* mean field method for atoms and molecules is the Hartree-Fock (HF) self-consistent-field (SCF) method. The total wave-function $\Psi(\mathbf{r}_1,\mathbf{r}_2,\ldots\mathbf{r}_N)$ of an electronic system, according to the exchange symmetry (and the general Pauli principle) for a system of N identical fermions (electrons) is an anti-symmetric linear combination (sum) of products of one-electron wave functions (orbitals) $\varphi_i(\mathbf{r}_i)$. This anti-symmetric linear combination of electronic orbitals is a NxN determinant $\overline{D}$ (known as Slater determinant) of the form:

$$\Psi(\mathbf{r}_1,\mathbf{r}_2,\ldots\mathbf{r}_N) \equiv \bar{D} = \frac{1}{\sqrt{N!}}\begin{vmatrix} \varphi_1(\mathbf{r}_1) & \varphi_1(\mathbf{r}_2) & \ldots & \varphi_1(\mathbf{r}_N) \\ \varphi_2(\mathbf{r}_1) & \varphi_2(\mathbf{r}_2) & \ldots & \varphi_2(\mathbf{r}_N) \\ \vdots & \vdots & \vdots & \vdots \\ \varphi_N(\mathbf{r}_1) & \varphi_N(\mathbf{r}_2) & \ldots & \varphi_N(\mathbf{r}_N) \end{vmatrix}. \quad (2)$$

The HF method, by its nature, does not include correlation effects due to the correlated (coupled) motion of individual pairs (or triplets, or quartets) of electrons. The difference of the HF energy from the actual energy of a system of electrons is by definition the correlation energy of the system. For many practical applications the HF results are not adequate and they are considered only as starting point of higher level perturbational or variational theoretical methods. The many-body perturbation expansion (with perturbation potential, the difference of the actual and average potentials) is known as Møller-Plesset (MP) perturbation theory. For many purposes second order Møller-Plesset (MP2) perturbation theory is adequate, although energies are usually calculated at fourth (MP4) and sometimes fifth (MP5) order, with a dramatically increasing computational cost, affordable only for small-size systems. The variational approach is based on the construction of a linear combination of several reference Slater determinants, i.e. 'multi-reference' (MR) wave functions, instead of one used in the HF method. These determinants can be constructed by combining occupied and virtual electronic configurations in conjunction with the 'configuration interaction' (CI) method. The full CI method is practically limited to very small molecules; this is why several variations and approximations of the MR and CI methods exist. These variants of MR and CI methods usually involve restrictions of the number and/or type of electronic configurations involved, e.g. singlets (S), doublets (D), triptlets (T), quadruples (Q), etc. The many-body approach to the electronic structure of atomic systems, depending on the type of the system and the desired quantity, includes several other methods, such as the coupled cluster (CC) method, the quadratic CI (QCI), as well as the restricted (R) and complete (C) active space (AS) methods; i.e. RAS and CAS respectively. Several variations and combinations of the many-body methods (both variational and/or perturbational) exist in the literature. These 'combined' methods are designed to optimized the accuracy (and in part the computational cost) of specific (more or less) calculations, under special conditions or assumptions applied to these particular cases. For time-dependent properties, such as optical absorption or emission, time-dependent (TD) versions of several of the above-mentioned methods exist, dealing with, instead of Eq.(1), the time-dependent Schrödinger equation:

$$\left\{-\frac{1}{2}\sum_{i=1}^{N}\nabla_i^2 + \sum_{i=1}^{N}\upsilon(\mathbf{r}_i) + \frac{1}{2}\sum_{i=1}^{N}\sum_{\substack{i=1\\(j\neq 1)}}^{N}\frac{1}{|\mathbf{r}_i-\mathbf{r}_j|}\right\} \cdot\Psi(\mathbf{r}_1,\mathbf{r}_2,\ldots\mathbf{r}_N,t) = i\frac{\partial\Psi(\mathbf{r}_1,\mathbf{r}_2,\ldots\mathbf{r}_N,t)}{\partial t}. \quad (3)$$

Apparently the computational cost is much higher for TD methods, compared to the corresponding 'static' ones. Several of the combined methods are equivalent with others at some level of approximation. Most of these methods (combined and single) are available in customized and widespread packages. As it is illustrated schematically in diagram 1, the decision of what method is more appropriate for a specific many electron system is not always easy or trivial. The answer depends strongly on the system and in particular on the structure of the ground and (low) excited states. Thus, the routine or 'black box' implementation of these high level techniques should be avoided as much as possible, because it could produce erroneous or misleading results. Furthermore the implementation of any high level method involves also several other technical approximations and details which only a knowledgeable person can decide if the results are going to be meaningful. The choice of the most suitable technical approximations (such as the quality and size of the basis set) after the choice of the most suitable *ab initio* method is very important for a desired accuracy at a given computational cost. For most of the applications on nanoclusters or nanocrystals, the majority of the many-body high-level methods described here are not applicable, if the size of the systems is larger than a few tenths of atoms. A good compromise, without resorting to empirical or semi-empirical techniques is the density functional theory (DFT), which in its simplest approximation is known as the local density approximation (LDA). The DFT, which offers an accurate description of larger systems with current computational power, is a mean-field theory which in principle is exact. In DFT the total energy (Hamiltonian) of the system is expressed in terms of a quantity known as 'the exchange and correlation energy functional', which is a unique functional of the electronic density $\rho(\mathbf{r}_1,\mathbf{r}_2,\ldots,\mathbf{r}_N)$. However, the exchange and correla-

Real Space High Level Theoretical Techniques

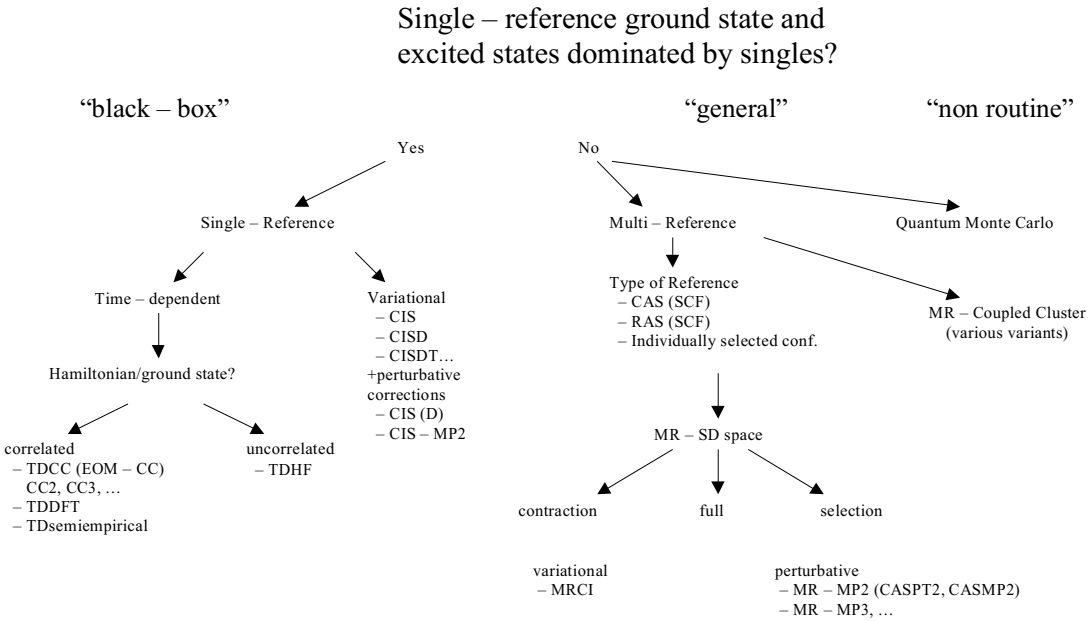

Diagram 1. A chart of the various real space high-level theoretical techniques, displaying their evolution and interrelation as well as the decisions involved in selecting one of them.

tion energy functional is unknown and has to be approximated in practice. Several well known functionals for exchange and correlation have been proposed in the literature. These functionals are used extensively in many atomistic and 'crystalline' calculations, with very good results. Unlike HF, the DFT includes correlation in a good approximation. The same is true for exchange, which however in HF is included exactly (not approximately). Relatively recently [48] hybrid DFT, HF schemes have been used which combine the advantages of DFT (accurate correlation) and HF (exact exchange). The most famous hybrid functional is the B3LYP functional [48] which has been very successful in realist calculations of materials properties (see reference [7] and references therein). The time-dependent DFT (TDDFT) [30,47] method has been proven extremely accurate for time-dependent and excited states properties, such as optical absorption and PL [7,30]. It should be emphasized at this point that an accurate description of the optical absorption or even the optical gap (which corresponds to optical absorption up to the first allowed excited state) requires a very good level of correlation in both the ground and the excited states. Thus the accurate evaluation of the optical gap (or the absorption spectrum) demands high level multi-reference and/or time-dependent theoretical techniques. A zeroth order crude approximation of the optical gap is the energy difference the highest occupied (HOMO) orbital from the lowest unoccupied (LUMO) orbital. This is a by-product of the ground-state calculation. The HOMO-LUMO gap for an infinite crystalline solid corresponds to the usual band gap, calculated by usual (mean field) band structure calculations. Sometimes a slightly better approximation, known as ΔSCF method, is used as a computational compromise between the high-level (TD) and the zero level (HOMO-LUMO gap). Instead of a TD calculation, two ground-state calculations are performed (one for the ground and one for the 'pseudo-excited' state and their energy difference is considered as the corresponding excitation energy. According to the ΔSCF method an electron is removed from the HOMO and placed in the LUMO orbital and the energy is recalculated. However, this is not a correct or accurate procedure, even when the ground-state calculations are of relatively high level.At least for the case of DFT calculations the ΔSCF procedure implies that the resulting excited state is a spin triplet. As a result, if total energy differences between the excited and ground states are consid-

Table 1. Comparison with experiment of the theoretical optical gap of some Si-H molecules, obtained by simple (from left) and complex (to right) theoretical techniques. The numbers in parenthesis correspond to results obtained with the larger basis set cc-PVTZ.

Si-H system	HOMO-LUMO (eV) HF	B3LYP	ΔSCF (eV) HF	B3LYP	ε_g Eq.(4)	CIS B3LYP	QMC ΔSCF	GW	TDDFT B3LYP (eV)	Exp (eV)
SiH_4	17.8 (17.1)	11.0 (10.5)	10.3 (9,8)	9.0 (8.8)	8,6	9.1 (8.8)	9.2	9.0	8.8	8.8
Si_2H_6	14.7	8.6	7.4	7.0	7.1	7.5	7.3	7.6	7.6	7.6
Si_5H_{12}	13.4	7.6	6.6	6.2	6.4	6.0	6.8	6.0	6.6	6.5

ered as optical absorption energies, then they correspond to singlet-triplet transitions. These transitions are spin forbidden unless there is a strong spin-orbit coupling. Moreover, removing an orbital from HOMO and placing it in LUMO does not necessarily mean that we have constructed a real excited state. Electronic transitions are meant to be transitions between states not between orbitals. As we can see in Table 1, by improving the quality of the ground-state calculations the quality of the ΔSCF gap improves (compare the results in Table 1 for HF and DFT/B3LYP, or the results for different basis sets). The difference between the HOMO-LUMO and the optical gap is termed the quasi-particle or the exciton self energy, which is usually approximated by the Coulomb screened electron–hole interaction E_{coul},

$$\varepsilon_g^{opt} = \varepsilon_g^{H-L} - E_{coul}, \tag{4}$$

where:

$$E_{coul} = \int \frac{|\Psi_H(1)|^2 \times |\Psi_L(2)|^2}{\varepsilon_\infty^{nanocr} |\mathbf{r}_1 - \mathbf{r}_2|} d\mathbf{r}_1 d\mathbf{r}_2 . \tag{5}$$

The nanocrystal dielectric constant, $\varepsilon_\infty^{nanocr}$ in Eq.(5) is usually approximated by empirical size-dependent expressions [30]. As we can see from Eq. (4), the HOMO-LUMO gap ε_g^{H-L} is always larger than the optical gap. On the other hand, the ΔSCF gap underestimates the optical gap (see Table 1 and Table 2 below). Thus the HOMO-LUMO and the ΔSCF gaps provide upper and lower bounds, respectively to the real optical gap. In Fig. 1 the real optical gap ε_g^{opt} is located somewhere in the shaded region between the two gaps. Evaluation of the screened Coulomb integral from Eq. (5) provides an alternative low-cost ground-state evaluation of the optical gap, which is both conceptually and computationally a much better approximation than ΔSCF and HOMO-LUMO gap [30]. This technique, with the advent of modern computational techniques (and computational resources) has become obsolete, although estimates of ε_g^{opt} based on this method for very small Si:H 'nanocrystals'-molecules are pretty good (see Table 1). Coming back to the high level *ab initio* techniques applicable to materials properties we should mention two new accurate and popular many-body techniques. One is a perturbative approach based on the solution of the Bethe-Salpeter equation within the GW-approximation [8]. This method, although time-consuming, is very promising especially for excited states and optical absorption. The second of the two many-body approaches [50], known as 'quantum Monte-Carlo' (QMC) is suitable for accurate ground-state calculations (and ground-state properties). This method

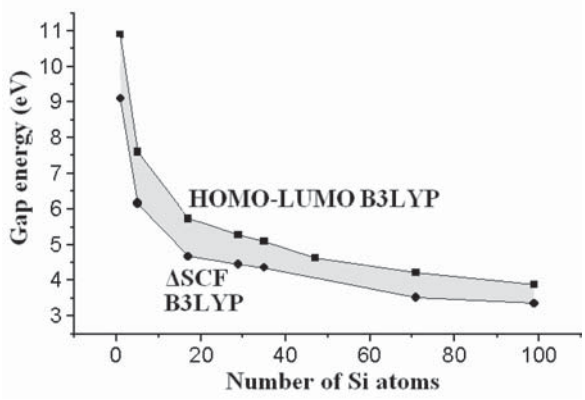

Fig. 1. Approximation of the optical gap, versus nanocrystal-size through simple (low-level) ground-state techniques: HOMO-LUMO gap and ΔSCF. The real gap is in the shaded region between the two curves.

Table 2. Comparison of the optical gap of the smaller nanocrystals with 5-35 Si atoms (#Si=5-35, #total=17-71) according to low (HOMO-LUMO gap, ΔSCF/B3LYP), medium (mixed high and low: ΔSCF/QMC) and high level (CIS/HF, TDDFT, MR-MP2) theoretical techniques.

#Si	HOMO--LUMO B3LYP	ΔSCF B3LYP(eV) (eV)	ΔSCF QMC (eV)	CIS/ HF (eV)	CIS/ B3LYP (eV)	TDDFT/ B3LYP (eV)	MR-MP2 (eV)	TTDFT/ BP86 (eV)
5	7.60	6.20*	6.9*	6.58*	6.05*	6.66*	6.56*	6.10*
17	5.72	4.68	5.7	5.46	5.25	5.03	5.01	4.44
29	5.15	4.40	5.2	5.44	5.01	4.53	4.45	3.85
35	5.04	4.36	5.0	5.33	4.93	4.42	4.33	3.73

*Experimental value: 6.5 eV.

is based on a completely different philosophy. The main idea of QMC is to model the many-electron wave function $\Psi(\mathbf{r}_1,\mathbf{r}_2,...\mathbf{r}_N)$ (and therefore the probability distribution $|\Psi(\mathbf{r}_1,\mathbf{r}_2,...\mathbf{r}_N)|^2$) using the computer to generate sets of random positions distributed in exactly the same way as the results of an idealized measurement. The average of many such computer experiments will provide the quantum mechanical expectation values, given the form of the many-body wave functions, through the well-known Metropolis algorithm. However, the wave functions $\Psi(\mathbf{r}_1,\mathbf{r}_2,...\mathbf{r}_N)$ are unknown many-body (10^{23}) functions, which have to be (drastically) approximated using trial wave functions which will be further optimized through the variational method. The usual form of the trial wave functions Ψ_T is of the Slater-Jastrow type:

$$\Psi_T = \overline{D}^{\uparrow}\overline{D}^{\downarrow}\exp\left[-\sum_{i>j}u(r_i,r_j)+\sum_i \chi(r_i)\right], \qquad (6)$$

where $D^{\uparrow}$ and $D^{\downarrow}$ are Slater determinants of the form of Eq. (2) of spin-up and spin-down electron orbitals obtained from HF or DFT calculations, and u and χ are suitable functions optimized by the variational principle [50]. A much better alternative of the variational QMC method, described above, is the *diffusion QMC*, which is based on the imaginary-time Schrödinger equation:

$$\left\{-\frac{1}{2}\sum_{i=1}^{N}\nabla_i^2+U(\mathbf{r}_1,\mathbf{r}_2,\ldots,\mathbf{r}_N)\right\}\Psi(\mathbf{r}_1,\mathbf{r}_2,\ldots,\mathbf{r}_N,\tau)= -\frac{\partial\Psi(\mathbf{r}_1,\mathbf{r}_2,\ldots,\mathbf{r}_N)}{\partial\tau}. \qquad (7)$$

This equation is identical to the time-dependent Schrödinger equation Eq. (3) when τ is replaced by the imaginary variable *it*. The imaginary time is just a mathematical trick which allows us to convert an arbitrary starting state $\Psi(\mathbf{r}_1,\mathbf{r}_2,...\mathbf{r}_N,\tau=0)$ into the ground state in the limit $\tau\to0$, without assuming any particular functional form, as we did in Eq. (6). As long as the starting state $\Psi(\mathbf{r}_1,\mathbf{r}_2,...\mathbf{r}_N,\tau)$ is not orthogonal to the ground-state wave function, in the limit $\tau\to0$ the function $\Psi(\mathbf{r}_1,\mathbf{r}_2,...\mathbf{r}_N,\tau)$ becomes proportional to the true ground-state wave function. We can see that if the potential $U(\mathbf{r}_1,\mathbf{r}_2,...\mathbf{r}_N)$ is ignored, Eq. (7) is just a diffusion equation describing a population of 'random walkers' diffusing in a 3N-dimensional configuration space'. If the 'kinetic energy' (Laplacian) term is ignored we have a rate equation describing radioactive decay. Thus Eq. (7) describes walkers diffusing in 3N-dimensional space while dying out or multiplied at a rate determined by the value of the potential $U(\mathbf{r}_1,\mathbf{r}_2,...\mathbf{r}_N)$. After a long time τ (theoretically infinite) the density of diffusing walkers becomes proportional to the ground state wave function $\Psi(\mathbf{r}_1,\mathbf{r}_2,...\mathbf{r}_N)$. Thus we have a simple physical picture which leads directly to a clever and efficient simulation algorithm for finding the ground-state wave function (and energy, as well) for thousands of electrons. For instance the cohesive energy of crystalline Ge (ground-state property) calculated with the diffusion QMC, coincides with the experimental value of 3.85 eV/atom, whereas the corresponding LDA (not DFT) value is 4.59 eV/atom. We should mention here that the comparison of the cohesive energy (ground-state property) calculated by QMC and LDA methods, is not a representative result of the DFT method. The LDA is restricted to the local density approximation, which does not include gradient (or 'pseudo-non-local') corrections in the exchange and correlation functional. This is the usual

distinction between LDA and DFT. In addition to gradient corrections, the B3LYP method includes the (partially) exact exchange, not implemented in this (exact) way in other functionals, such as the BP86 [49] results of which are listed inTable 2. As we can see in Table 2, the exact exchange is very important for the correct description of the optical gap (excited-state property), since the values of the gap obtained by BP86 are much lower (about 0.5 eV) than the accurate MR-MP2 results. Also, the accurate exchange seems to be especially important (due to quantum confinement) for small nanocrystals. It is clear therefore that the diffusion QMC is a high- level accurate ground-state method. Its use for excited states or optical gaps is only implemented through one the simple ground-state crude (more or less) approximations, such as ΔSCF (see results in Table 1). The accuracy of such calculations is haphazard and cannot be taken for granted. Therefore this type of calculations which combine a very high-accuracy ground-state method with another low-level (and low-accuracy) ground-state method [23] could lead to misleading conclusions about the optical gap (which is an excited-state property). After all, as we can see in Tables 1 and 2, the ΔSCF/QMC accuracy is not better than that of the corresponding ΔSCF/B3LYP results. Furthermore, the ΔSCF/QMC results of Ref. [23b] are in conflict with truly high-level high-accuracy *ab initio* MR-MP2 (as well as and TDDFT/B3LYP) results [7], listed in Table 2. Up to now we have concentrated in *ab initio* theoretical methods (e.i. methods without arbitrary adjustable parameters). This overview would be incomplete without a few comments about empirical and semi-empirical techniques (involving adjustable parameters) which are very popular and widespread. In the most general meaning of the term, besides the 'classical' extended Hackel, MNDO and the various force fields, empirical methods encompass a variety of effective mass and tight-binding (TB) methods, both in real space (e.g. tight-binding molecular dynamics) and in k-space (e.g. TB super-cell). These methods are absolutely indispensable in science and in technology due to their simplicity, efficiency (low computational cost for large systems portability) and transparency (most of the times, but not always). For example for Si nanocrystals most of high level *ab initio* methods cannot deal readily with nanocrystal sizes larger than 2.5-3 nm; whereas the empirical techniques can easily and efficiently describe relatively large nanocrystals, encountered in many nanotechnology, nanoelectronics and microelectronics applications. However, for sizes of (practically) zero (quantum dots) and infinite (crystallites) extent where high correlation and accuracy *ab initio* calculations are possible, the phenomenological parameters should be properly adjusted in order to reproduce the high level *ab initio* results. If this is not done, these calculations should be considered with great caution, since the fitting of the parameters to bulk sizes, may not reproduce correctly the effect of the quantum confinement, which is very important for such small nanocrystal sizes. After all, the same parameters cannot usually describe much more properties from those which they were designed for. Finally, caution should be also exercised (for the compatibility of the parameters) when empirical techniques are combined with higher level methods of correlation, such as perturbation theory or configuration interaction (CI).

Closing this general overview of the theoretical methods we should make a final and general comment independent of the type and level of the theoretical techniques about the so called 'geometry optimization' or 'relaxation'. Geometry optimization is the process through which the equilibrium positions of the atomic nuclei are specified, within a given symmetry restriction. In most of the cases the geometry optimization is absolutely necessary since the exact position of the atoms, which enter parametrically the electronic Hamiltonian (within the adiabatic approximation) are not known exactly. Thus, geometry optimizations, which involve the calculation of forces (gradients of the energy with respect to nuclear coordinates) in addition to the calculation of energies are an essential ingredient of most of the calculations. Of course, these calculations are performed within the adiabatic or the Born-Oppenheimer approximation. In more complex cases the electron-atomic vibration interaction should be taken into account someway. The simplest manifestation of electron-vibration interaction is the Jahn-Teller effect which results in permanent distortions of highly symmetric structures. In view of the fact that that the calculation of gradients is more expensive and time-consuming, most of the times the geometry optimization, i.e. the calculation of forces (and the repetition of this procedure until the total force vanishes within some limits) is performed with a lower-level method or technique than the calculation of energies. For instance, a few years ago, calculation of forces at the HF level with the corresponding calculation of energy at the MP2 level or higher (and perhaps with a better basis set), was not unusual. Nowadays MP4 and QCI optimizations are almost trivial, but for very small molecules or nanoclustres. The B3LYP method offers

an attractive alternative for a consistent and accurate calculation of both forces and energies at the same level for much larger molecules and nanoclusters.

3. OUTLINE OF THE CALCULATIONS

The general theoretical and computational framework of the Patras work has been discussed briefly in the previous section, as part of the general overview. Most of the remaining general computational details are given in the published and to be published work [7, 30, 31, 35, 37, 41]. The diameter of the larger nanocrystal studied here, falls in the range of 12-24 Å. In this range of diameters visible photoluminescence has been reported. All nanocrystals have T_d symmetry and their geometries have been fully optimised within this symmetry constrain using the B3LYP exchange-correlation functional [48]. In Fig. 2, the geometrical structure of some representative Si nanocrystals is shown in 'ball-and-stick' diagrams. The number of silicon atoms in the nanocrystals ranges from 1 to 281. The number of hydrogen atoms varies from 4 to 172 atoms (thus, the larger nanocrystal contains a total of 453 atoms). Finally, the number of oxygen atoms in the nanocrystals containing oxygen varies from zero up to 24. These nanocrystals have been prepared by a special substitution procedure of surface hydrogen atoms in order to maintain the T_d symmetry of the initial oxygen-free nanocrystals. The starting point was a pre-selected set of surface Si atoms bonded to hydrogen for each of the hydrogen passivated nanocrystals. Each selected silicon atom has a bonding scheme of the form RNSi2{Si}H2. In this notation, RN is the main body of the nanocluster, Si2 are the two silicon atoms bonded to this particular atom {Si}, and H2 are the two hydrogen passivants. In addition to the selected Si atoms, we select also all symmetry equivalent Si atoms and replace in all of them the two hydrogens by one doubly bonded oxygen atom. For the selected sites the bonding scheme changes to RNSi2{Si}O. The bonding hybridization of the{Si} atoms changes from sp^3 to sp^2. It is also clear that for these nanocrystals the number of the surface oxygen atoms is dictated by the need to maintain the T_d symmetry. Thus, we have considered only the $Si_{17}H_{12}O_{12}$, $Si_{29}H_{12}O_{12}$, $Si_{35}H_{24}O_6$, $Si_{47}H_{48}O_6$, $Si_{71}H_{72}O_6$, $Si_{99}H_{76}O_{12}$ and $Si_{147}H_{52}O_{24}$ nanocrystals with double Si=O bonds. However, we also constructed two additional nanoparticles ($Si_{47}H_{36}O_{12}$ and $Si_{71}H_{60}O_{12}$), in which the surface oxygen atoms form a bridge between two Si atoms (instead of being doubly bonded). For $Si_{47}H_{36}O_{12}$ we have also constructed a variant, $Si_{47}H_{24}O_{18}$, which contains both bridging bonds Si-O-Si and double bonds Si=O, see Fig. 2c. The DFT and the TDDFT calculations for all nanocrystals (Si, Ge, SiGe) were performed with the TURBOMOLE [51] suite of programs using Gaussian atomic orbital basis sets of split valence [SV(P)]: [4s3p1d]/2s [52] quality which involves 5400 basis functions for the largest Si systems studied. The TDDFT calculations have been performed as described in detail in Ref. [53] using the B3LYP functional consistently for both, the self-consistent solution of the Kohn-Sham equation for the ground state, and the solution of the linear response problem. The MR-MP2 calculations have been performed as described in Ref. [54]. As, we have mentioned in the previous section, the (partially) exact Hartree-Fock (HF) exchange is especially important for 'confined' small size nanocrystals. Furthermore, the inclusion of exact HF exchange remedies the well-known deficiency of local-density approximation (LDA) to underestimate the band gap (and overestimate the cohesive energy). For the case of Si_6 cluster we have used also correlation consistent cc-pVTZ basis sets of triple-Z quality, and in addition to the MR-MP2 method we have used quadratic CI (QCI, QCISD(T)) and coupled clusters CCSD(T) methods employing both cc-PVDZ and cc-PVTZ basis sets [46].

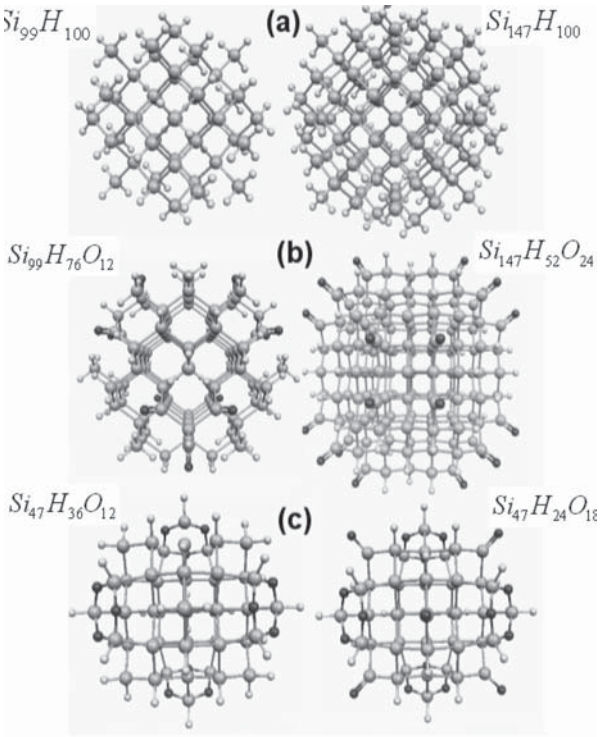

Fig. 2. Geometrical structure of representative silicon nanocrystals in 'ball-and-stick' diagrams.

4. RESULTS AND DISCUSSION FOR THE SILICON NANOCLUSTERS

4.1. The optical gap

In Fig. 3 our high accuracy [7] theoretical (TDDFT/B3LYP) results for oxygen-free silicon nanocrystals are presented and compared with several other theoretical and experimental results. In the same figure we have also included our TDDFT/BP86 results for comparison. As we have mentioned earlier the BP86 functional, which unlike B3LYP does not include the (partially) exact exchange, underestimates the optical gap by about 0.5 eV on the average. In Fig. 4 we summarize our results for both oxygen-free and oxygen-rich nanocrystals and we compared them with the corresponding (high accuracy) experimental results of Wilcoxon *et al.* [2]. The same results for nanocrystals with more than 35 Si atoms are tabulated in Table 3, as an extension of Tables 1 and 2. As we have mentioned in section 2 and elsewhere [7, 30], the differences between theoretical results depend strongly on the type and level of calculations (ab initio or phenomenological, real or *k* space) and the treatment of correlation and exchange. For the majority of the phenomenological calculations, the existing differences are attributed to 'problematic' choice of the phenomenological parameters from bulk values without proper account of confinement. The discrepancies between high level ab initio calculations, as we pointed out in the previous section, are due to either inconsistencies in the secondary approximations and methods (of lower level) or in poor treatment of exchange and (to a lesser degree) of correlation. The accurate treatment of the exchange interaction is unexpectedly important for small nanocrystals. We have verified this by performing in parallel with the TDDFT/B3LYP, calculations with the non-hybrid BP86 functional [49], which treats exchange in a lower level than B3LYP. As we have seen in Table 2, the gap is underestimated by the BP86 functional by 0.5-0.6 eV. The same trend of gap underestimation holds true for both oxygen-free and oxygen-rich nanocrystas. The agreement with experimental data in Figs. 3 and 4 is in general very good. As we have illustrated earlier [7], the apparent disagreement with some of the experimental data, especially those assumed to be oxygen free, is mainly due to experimental difficulties in the size determination and/or to oxygen contamination of the samples. The oxygen 'contaminated' samples are lying, according to Wilcoxon *et al.* [2], in the shaded region of Fig. 4. As we can see in this figure all of our oxygen-rich results fall inside the shaded region. Wilcoxon *et al.* have demonstrated that all experimental results inside the shaded area of the figure are oxygen contaminated either by exposure to air or by the size regulating oxidation process. Wolkin *et al.* [3] have demon-

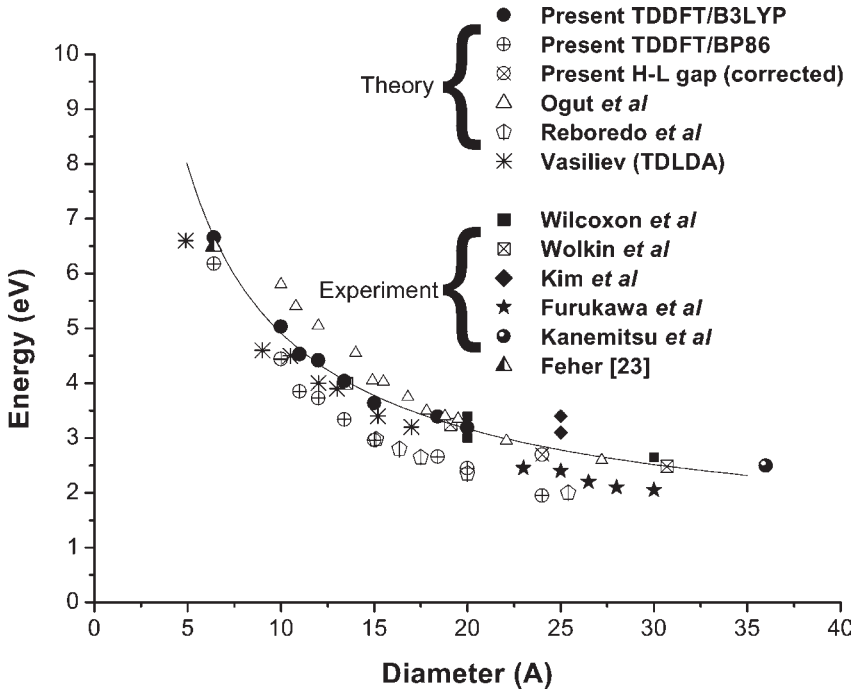

Fig. 3. Comparison of our high-level theoretical results for the optical gap versus the diameter of oxygen-free silicon nanocrystals with a variety of theoretical and experimental results.

Table 3. The optical gap (E_g) obtained with TDDFT/B3LYP for larger nanocrystals with 47 up to 147 silicon atoms, 60-100 hydrogen atoms and 0-24 oxygen atoms. The HOMO-LUMO gap for oxygen-free nanocrystals (H-L) is shown for comparison.

#Si	# H	H-L/ B3LYP (eV)	E_g(TDDFT) B3LYP (eV)	#H	#O	E_g(TDDFT) B3LYP (eV)
47	60	4.64	4.04	48	6	2.70
47	–	–	–	36*	12*	3.7*
71	84	4.20	3.64	72	6	2.21
71	–	–	–	60*	12*	3.1*
99	100	3.89	3.39	76	12	2.45
147	100	3.66	3.19	52	24	1.85
281	172	3.11	2.61	–	–	–

*Only bridging Si-O bonds. No double bonds.

strated that even a 3 min exposure of the samples in air produces a red shift as large as 1 eV (for relatively large nanocrystals) due to the formation of oxygen bonds. Our calculated red-shift ranges from about 2 eV, for the smaller, down to 1-1.3 eV, for the larger nanocrystals considered here, in full agreement with Wolkin et al [3]. The results inside the shaded region of Fig. 3 incorporate different amounts and different distributions of oxygen for the same number of Si atoms. Therefore, it is difficult to join them with a continuous line. In order to investigate the dependence of the optical gap on the amount and distribution of surface oxygen, we have first altered the number of surface oxygen atoms without altering significantly their environment. This was accomplished by keeping their relative positions unchanged (for instance the same interatomic distance between oxygens, around 3.8 Å). Technically, the construction was carried out by a careful selection of the oxygen atoms to be removed, so that the remaining oxygen atoms keep the (lower) symmetry of the resulting nanoparticle as high as possible. This procedure was carried out only for the $Si_{29}H_{12}O_{12}$ nanocrystal. The changes of the optical gap (not of the entire absorption spectrum) in this case were marginal. However, when the same changes of the number of oxygen atoms were implemented without any precautions to preserve the bonding environment (for instance with an increased oxygen separation) we obtained (fundamental) optical gaps blue-shifted by as much as 0.45 eV. Thus the critical parameter for the change of the gap is not just the amount of oxygen but the bonding environment and the way the oxygen atoms are accumulated on the surface (i.e. the surface chemistry). In any case, for large amounts of oxygen concentration with a broad and dense distribution, small changes of the bonding environment are practically unnoticeable. A similar conclusion about the dependence of the gap on the amount of oxygen (and the bonding environment) was drawn by Puzder *et al.* [23] by examining the single particle HOMO-LUMO gap of a Si_{66} nanoparticle. In particular, the gap difference, observed by Puzder *et al.* between $Si_{66}H_{56}O_4$ and $Si_{66}H_{40}O_{12}$ was found to be in the range of 0.4 eV. This value, despite the fact that it corresponds to the single particle HOMO-LUMO gap (and cannot be trusted in general as a zeroth order quantity), its

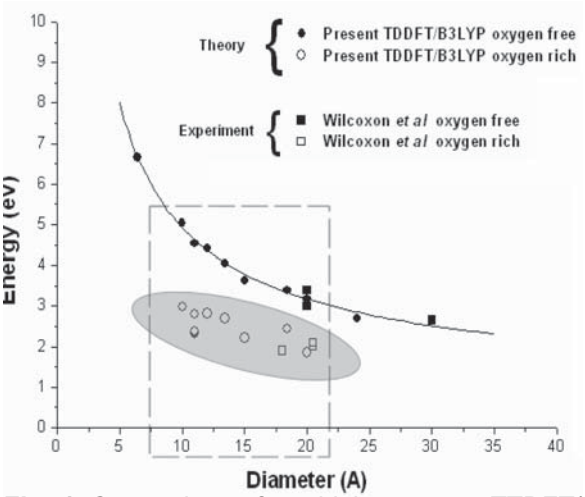

Fig. 4. Comparison of our high accuracy TTDFT/B3LYP theoretical results for oxygen-free and oxygen-rich silicon nanocrystals with the corresponding experimental results of Wilcoxon *et al*. [2]. The shaded area is designated by Wilcoxon et al as the region for oxygen-'contaminated' samples.

shift between two similar nanocrystals is in excellent agreement with our 0.45 eV shift of the (many-body) optical gap. This agreement of differences (not absolute values) could be understood if we accept that the trend of an almost constant difference between optical and HOMO-LUMO gaps observed for the oxygen-free, extends to the oxygen-rich, nanocrystals. Similar results of Puzder *et al.* [17] using a combination of quantum Monte Carlo and ΔSCF calculations, are in good agreement with our results for the relative changes of the gap, for apparently the same reasons. Several of the trends and qualitative assessments for the optical gap described here (with or without the investigation of their range of applicability) have been observed earlier in one form or another [18,27-29] for smaller nanocrystals. All of the results described so far for the oxygen-rich nanocrystals have been obtained assuming double-bonded silicon-oxygen atoms. In order to investigate the influence of this widely-used assumption we have examined for the Si_{47}:H,O nanocrystal variations in the oxygen bonding by including oxygen-silicon bridging bonds (Si-O-Si) in addition or instead of oxygen-silicon double bonds (Si=O). The two structures are shown in Fig. 2c. In both cases the optical gap is lowered by oxygen, compared to the oxygen free nanocrystal $Si_{47}H_{60}$. In the case of $Si_{47}H_{36}O_{12}$ with only bridging bonds the value of the optical gap (3.7 eV) still lies well above of the visible region of the spectrum. On the contrary, for the case of the $Si_{47}H_{24}O_{18}$ nanocrystal, which includes both double (Si=O) and bridging (Si-O-Si) oxygen bonds, the fundamental optical gap is red shifted down to 2.5 eV. Similar results were obtained for the $Si_{71}H_{60}O_{12}$ nanosystem. Thus, bridging bonds by themselves cannot lower the gap enough to get inside the visible region, in contrast to the Si=O double bonds. Finally, as an additional test of the influence of the bonding environment, we have performed additional calculations on the Si_{35} nanocrystal with the surface dangling bonds passivated by both hydrogen atoms and hydroxyl groups. Zhou *et al.* [27] have examined the same system and obtained a HOMO-LUMO gap of 2.73 eV, inside the visible region of the spectrum. Since the optical gap, as we have shown before, Eq. (4), is always lower than the HOMO-LUMO gap, this implies that with hydroxyl passivation the optical gap is red shifted in the visible. Indeed, our calculations for $Si_{35}(OH)_{36}$ give an HOMO-LUMO gap of 2.6 eV, in agreement with the conclusions of Zhou *et al.* [27]. However, when we examined partially 'hydroxylated' nanoparticles such as $Si_{35}H_{24}(OH)_{12}$ and $Si_{35}H_{34}(OH)_2$, the gap was increased by as much as 1.8 eV for $Si_{35}H_{24}(OH)_{12}$ and 2.2 eV for $Si_{35}H_{34}(OH)_2$. The new HOMO-LUMO gaps of 4.42 eV and 4.83 eV respectively, are well outside the visible region. In other words, we observe that the effect of hydroxyl passivation is largely dependent on the amount of hydroxyl groups deposited on the surface and probably on their spatial distribution. This observation takes us back to the role of relative positions of the oxygen atoms. The big difference between the behavior of hydroxyls and double-bonded oxygen is that, although a few (even 2 or 3) double-bonded oxygen atoms can reduce the optical gap below 3 eV, to accomplish the same reduction of the gap by hydroxyl a much larger amount of hydroxyls is needed. Therefore, the most appropriate and efficient reduction of the gap, in cases of small amounts of oxygen, is accomplished by double-bonded oxygen 'contaminants'. Thus, the visible PL observed recently [24] from nanoparticles with diameters around 1 nm, must be due to oxygen 'contamination' of the samples, since the only oxygen-free nanocrystals in this range of diameters are Si_{29} and Si_{35}, which according to Table 2 and Figs. 3 and 4 have optical gaps of 4.5 and 4.4 respectively. The reported experimental value of the optical gap by Ackakir *et al*. [24] is 3.5 eV. This value would be consistent with our calculations only if double-bonded oxygen atoms were present (even in very small numbers). This is indeed the case for both $Si_{29}H_{12}O_{12}$ and $Si_{35}H_{24}O_6$. As we can see in Fig. 5 below, the 3.5 eV peak is 'loud and clear'. What is even more important is that another very weak peak around 2.8 eV is also present and should be also observable if the experimental measurements are sensitive enough (we will come back at this point later). If, however, the presence of oxygen (even in very small amounts) is excluded, then alternative explanations should be pursued. Following this last approach, Mitas e*t al.* [25] performed ab initio Configuration Interaction Singlets (CIS) calculations on several reconstructed variants of Si_{29} nanoparticle. As we can see in Table 2, the CIS/HF overestimates the optical gap and therefore is not always accurate. In order to correct the overestimation of the gap produced by the simple CIS calculations Mitas *et al*. [25] calibrated the CIS results with the help of selective Quantum Monte Carlo calculations. Their calibrated results for the $Si_{29}H_{24}$ reconstructed cluster show indeed an optical gap with the desired value of 3.5 eV. Therefore, $Si_{29}H_{24}$ was proposed as a candidate for the experimentally observed luminescence [24]. However, Mitas *et al.* [25] did not examine at any point of their work the structural stability of these reconstructed nanoparticles. For this reason we

have performed an additional DFT/B3LYP geometry optimization on the reconstructed $Si_{29}H_{24}$ nanocluster in order to compare its binding energy with the corresponding binding energy of our $Si_{29}H_{36}$ nanocluster. Actually, due to the fact that the two nanoclusters contain a different number of hydrogen atoms, we can only compare the calculated binding energies per silicon atom (or compare the energies of $Si_{29}H_{36}$ and $Si_{29}H_{24}$+ $6H_2$, in the worst case scenario for $Si_{29}H_{36}$). No matter which of the two methods is used, our results show that the $Si_{29}H_{36}$ structure is energetically more favorable compared to the structure of $Si_{29}H_{24}$ (by as much as 1.7 eV per Si atom with the first method). We consider the difference of 1.7 eV per Si atom too large to be disregarded. If, however, despite this large energy difference, the $Si_{29}H_{24}$ structure is still considered responsible for the optical absorption, then it should be also proposed under what conditions this structure becomes energetically favourable compared to $Si_{29}H_{36}$. We believe that this is highly improbable, in view of the preparation procedure, described by Akcakir *et al.* [24], according to which 'the hydrogen passivation was more complete and of better quality compared to other hydrogenated nanocrystals'. In an environment full of hydrogen with more effective hydrogen passivation, we believe that the suggestion of $Si_{29}H_{24}$ formation instead of the energetically favourable (and with more complete H passivation) $Si_{29}H_{36}$ structure, is highly questionable. Since oxygen contamination, in very small amounts, cannot be ruled out, even in hydrogen rich environments, we propose that the observed peak at 3.5 eV is due to double-bonded oxygen atoms (even in very small amounts). As we have mentioned earlier, if this is the case, we should also expect a much weaker peak around 2.8 eV. Indeed, this is the case. As we found out in the literature, the experimental results of Akcakir *et al.* [24] and the theoretical calculations of Mitas *et al.* [25] have been recently expanded, re-examined and complemented with TDDFT calculations by Rao *et al.* [26]. As far as the experimental part is concerned, it is evident that for the (around) 1nm nanoparticles the lowest excitation energies are 3.7, 4.0, and 4.6 eV, while the authors also observe a weak emission peak around 2.8 eV.

This is in excellent agreement with our results for both $Si_{29}H_{24}O_4$ and $Si_{35}H_{24}O_6$ in figure 5. However, Rao *et al.* [26] claim based on existing literature at that time, that the observed optical properties of their samples could not be explained by means of oxygen contamination due to the presence of the 2.8 eV peak, which could not be explained by the theoretical results which they were known to them at that time. In view of our present calculations, we suggest that the experimental data of Akcakir *et al*. [24] as well as those of Rao *et al.* [26] are consistent with the hypothesis of oxygen contamination (even in very small amounts).

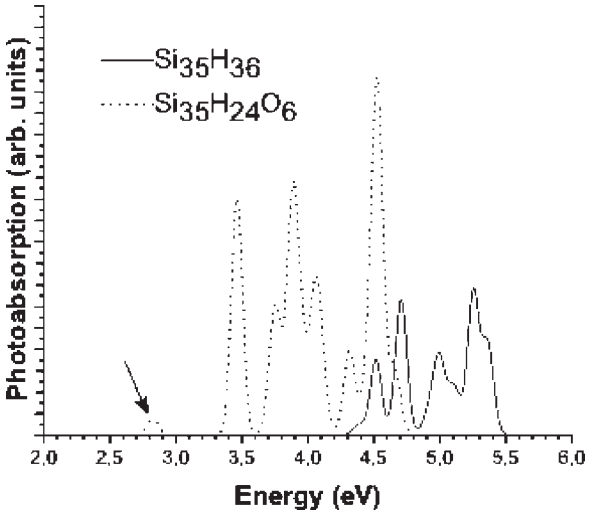

Fig. 5. Comparison of the absorption spectrum of oxygen-free and oxygen-rich silicon nanocrystals, for a small nanocrystal with diameter about 1.2 nm.

4.2. The excitation spectrum and density of states diagrams

In addition to the fundamental optical gap, we have also calculated (using TDDFT/B3LYP) the lowest twenty spin-and-symmetry-allowed excitations along with their corresponding oscillator strengths, for selected nanocrystals. In Fig. 5 we have plotted the lower part of the calculated absorption spectrum of the Si_{35} nanocrystal, with and without oxygen. This spectrum was obtained with a suitable broadening of the twenty calculated spectral lines. As we can see in Fig. 5, the presence of surface oxygen, not only affects the value of the fundamental optical gap, but it additionally produces a significant enhancement of absorbance (large oscillator strengths). This is due to the fact that both HOMO and LUMO orbitals are localized around oxygen sites, as we can see in Fig. 6, and their overlap is enhanced. As a result, the transition from HOMO to LUMO is reinforced due to the larger strength of the corresponding matrix element. At the same time, the localization of both HOMO and LUMO orbitals

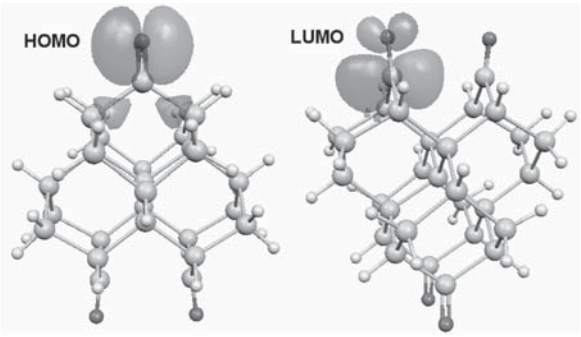

Fig. 6. The spatial distribution of the HOMO and LUMO natural orbitals, of $Si_{29}H_{28}O_4$ displaying the localization of these orbitals around double-bonded oxygen sites. The orientation of the nanocrystal is different in the two figures for clarity.

on oxygen sites shows that the gap is dominated and determined by oxygen double bonds, at least for small nanocrystals as Si_{35}. This is also clear from the corresponding density of states (DOS) in Fig. 7. Fig. 7 shows the energy level diagrams of $Si_{71}H_{84}$, $Si_{71}H_{72}O_6$ together with the corresponding density of states (DOS) diagrams, obtained from the eigenvalues of the ground-state calculations with a suitable gaussian broadening. In the same figure the DOS curves are shown for $Si_{35}H_{36}$, $Si_{35}H_{24}O_6$ (the absorption spectrum of which was given in Fig. 5) together with the DOS curves of a much larger pair of nanocrystals, $Si_{147}H_{100}$ and $Si_{147}H_{52}O_{24}$. We have, thus, a representative picture of the electronic structure for small, medium and large ('small') nanocrystals. As we can see, the presence of oxygen affects mainly the tail of the conduction band by inserting a new peak, dominated by oxygen. Consequently, the reduction of the optical gap is consistent with an analogous decrease of the HOMO-LUMO gap. We can easily see from these DOS plots that the oxygen related peak is located well within the gap (in the energy region of -3.4 eV). A less pronounced, but very important effect introduced by the presence of oxygen atoms is the change in the character of the valence band-tail. The valence band-tail of the two smaller oxygen-rich nanoparticles of Fig. 6 exhibits a fine structure which is due to localized double-bonded oxygen states. The relative energy position of these peaks facilitates the formation of localized stable Si=O bonds. Thus, for the small nanocrystal regime, where the gap is bigger due to stronger confinement, the oxygen related states do not overlap with the valence band. As a result, in this case, oxygen plays the key role in the determination of the optical properties of Si nanocrystals. As the size of the nanocrystal increases the band gap decreases and the oxygen peaks gradually overlap with the band tails. This can be clearly seen in Fig. 7 for the case of $Si_{147}H_{52}O_{24}$ nanocrystal. In this case the oxygen related states significantly overlap with the tail of the conduction band, while the valence band-tail

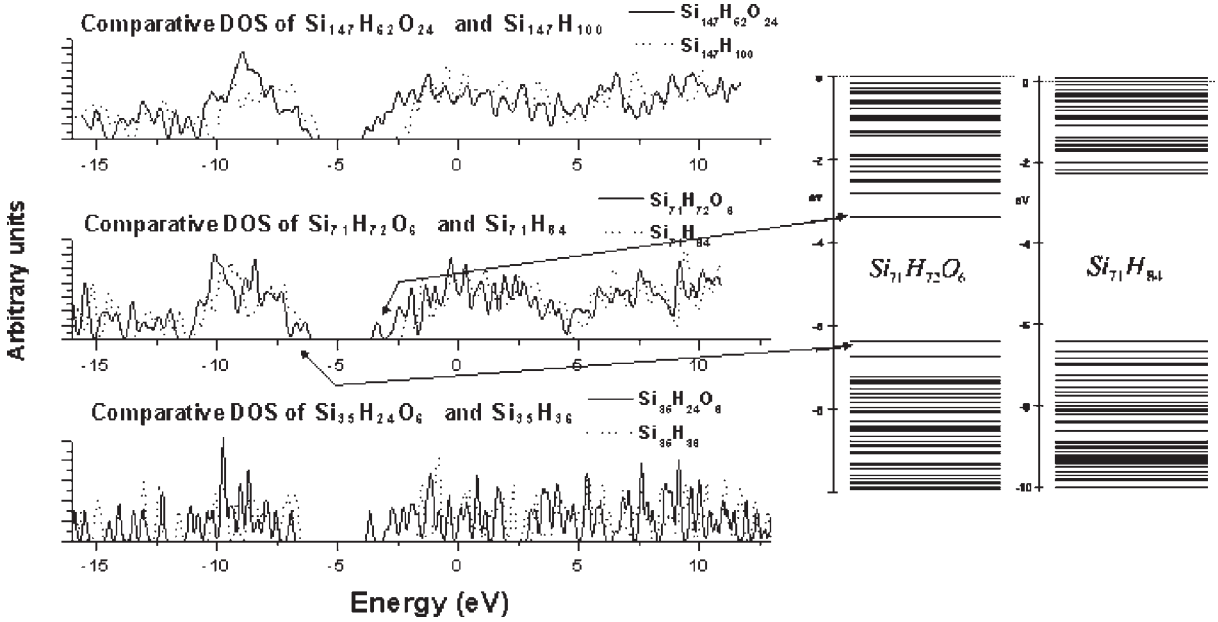

Fig. 7. Comparison of the energy-level diagrams and the corresponding density of states (DOS) of oxygen-free and oxygen-rich (hydrogen passivated) silicon nanocrystals of various sizes.

exhibits no fine structure. Thus, the Si=O bonds are destabilized for bigger nanocrystals and they can not even be formed. In this case oxygen serves as a simple passivant which no longer determines the optical properties of nanocrystal.

4.3. Discussion and summary for Si nanocrystals.

After all this discussion about the role of oxygen 'contamination', it becomes clear that the diverse (experimental and theoretical) conclusions for the variation of the optical gap versus nanocrystal size, and consequently for the minimum size for visible PL can very easily explained by the existence of doubly bonded oxygen atoms in the surface of the nanocrystals. The Si=O bonds can explain the 'minimum diameter' of 15 Å, suggested by Schuppler *et al.* [5] as well as the visible PL at 10-12 Å, (1-1.2 nm). Thus the true critical diameter in the presence of oxygen (and/or reconstruction) could be smaller than 10 Å. On the other hand, for oxygen-free nanocrystals, the critical dimension for light emission is significantly larger and well above than 20 Å (between 22 and 23 Å). As we can see, our results can actually bridge the differences in existing experimental (and theoretical) results. By extrapolating the optical gap of Fig. 2 for oxygen-free samples we can also estimate the maximum size of nanocrystals emitting in the visible region to be around 85 Å, if such extrapolation could be trusted. The values of the fitted parameters for the gap versus diameter in the limit of $d \to \infty$ suggest a band- gap value of 1.17 eV. This value is very encouraging for the suggested minimum and maximum critical diameters for visible PL.

5. RESULTS AND DISCUSSION FOR THE Ge:H AND Si-Ge:H NANOCLUSTERS

5.1. Germanium nanocrystals

The extension of research interest from Silicon to Germanium nanocrystals is rather straightforward [37], as both are group IV semiconductors. Furthermore, Ge has a smaller band gap than Si thus making it possible for smaller structures to produce visible PL. Experimentally PL has been observed in the range 350-700 nm from Ge nanocrystals 2-5 nm in size [32], while there are also studies concerning much larger nanoparticles [33]. It should be noted that up to date the optical properties of Ge quantum dots have been studied only in the framework of either semiempirical methods [34], or simple

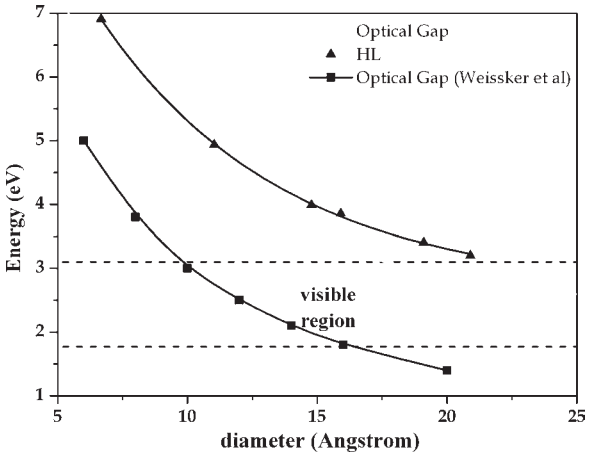

Fig. 8. The variation of the optical and HOMO-LUMO (HL) gap(s) with the diameter of oxygen-free hydrogen-passivated germanium nanocrystals. The ΔSCF/LDA theoretical results of Weissker *et al.* [35] are also displayed for comparison.

local density (LDA) ground-state calculations [35,36]. The geometries of Ge:H are completely similar with those of the corresponding Si:H nanocrystals in Fig. 2 (except the bond length). In Fig. 8, we have plotted the variation of both HOMO–LUMO gap (HL) and the fundamental optical gap as a function of the diameter of the Ge nanocrystals. The two curves, compared to the corresponding of Si nanocrystals, are shifted to lower energies but they have almost the same size dependence. The diameter of the smallest Ge nanocrystal for which the fundamental optical gap lies in the visible area of the spectrum is in the range of 19-20 Å, whereas the corresponding critical diameter for Si was 22Å. In the same figure we can see the LDA/ΔSCF results of Weissker *et al.* [35], which are significantly shifted from the real values to much smaller gap energies. This is not surprising since it is well known that simple LDA calculations, seriously underestimates the value of the HOMO-LUMO gap. Moreover, as we know from the discussion of section 2, the ΔSCF approximation tends to underestimate the optical gap. Consequently, the combination of the two approximations adopted by Weissker *et al.* unavoidably leads to a serious underestimation of the optical gap, which is also in conflict with the experimental results of Wilcoxon *et al.* [32]. Our results seem to have a better agreement with the LDA ground-state calculations of Melnikov *et al.* [36] This can be attributed to the fact that, the underestimation of single particle excitation energies de-

rived by ground-state LDA calculations is of the same order of magnitude with the exciton binding energy in our calculations. However, the agreement deteriorates when the authors subtract from their single particle energies the electron-hole (exciton) Coulomb interaction energy. Although this is physically correct, the LDA single particle transition energies are already underestimated and further subtraction of the exciton binding energy makes them worse. As in Si, the difference between the HOMO-LUMO gap and the fundamental optical gap can be considered to approximate the binding energy E_B of the exciton formed due to the electronic excitation. As expected by the quantum confinement hypothesis, E_B must decrease as the diameter of the nanocrystal increases. For diameters around 20 Å, the value of E_B is found to be approximately 0.45 eV. Compared to the case of Si nanocrystals, we see that although the Si and Ge nanoparticles with $d \approx 20$ Å contain different number of atoms, the values of E_B practically coincide. The first allowed transition of each nanostructure (fundamental optical gap) is found to have comparably large oscillator strength, which is consistent with the indirect to direct transition in the spectra of Ge nanostructures, as their sizes decrease. The direct nature of the fundamental optical gap becomes evident from the fact that the allowed transitions are between the HOMO and LUMO orbitals, in contrast to Si nanocrystals for which the HOMO-LUMO transition was always forbidden [7]. The larger nano-crystal in this work ($Ge_{99}H_{100}$) has an approximate diameter of 22 Å (including the surface hydrogen atoms) and its fundamental optical gap is at 2.65 eV. Although the size of this nanocrystal is still too small to compare directly with existing experiments, the value of 2.65 eV is in excellent agreement with the results and conclusions of Wilcoxon *et al.* [32], suggesting that the critical diameter of oxygen-free germanium nanocrystals is around 2 nm. Finaly, our results unambiguously verify the indirect to direct transition of Ge nanoparticles as their size decreases, showing that the HOMO-LUMO transition is both spin and symmetry allowed.

5.2. Mixed Si_nGe_m:H nanocrystals

The critical region of sizes (diameters) for visible PL in silicon nanocrystals extends from around 22 Å up to an estimated value of 85 Å. The corresponding critical region for germanium is smaller, starting from around 19 Å. Thus, porous silicon (composed of Si nanocrystals), Si or Ge nanocrystals by themselves, offer the possibility of intense tunable PL. By varying the diameters of the nanocrystals (or equivalently the porosity of porous silicon) intense PL can be obtained across the visible spectrum. This could never take place for bulk crystalline silicon or germanium with a band gap of 1.2 eV and 0.9 eV respectively. As it is understood by now, quantum confinement is responsible for the opening of the gap from the bulk value of 1.2 eV (for silicon) to values of 2-3 eV (for larger nanocrystals) or to 6-7 eV for smaller nanocrystals (see Figure 3 or Tables 2 and 3). This over-opening of the gap for small sizes is, obviously, equally undesirable as the shrinking of the gap (in bulk Si or Ge).This problem at small sizes is not so strong for Ge nanocrystals because of the smaller band gap of bulk Ge, compared to Si. Even in this case, the possibilities of adjusting the optical gap (and the band gap) are limited only to proper size selection. The possibility of combining the advantages of Si (not only in the optical, but also in the electronic and technologically useful properties) with those of Ge is an intriguing and very promising project. Needless to say, that it is not only the minimum critical diameter of the nanocrystals which is important (for visible PL) but also the maximum possible diameter. With this in mind, we have examined [39] the optical and electronic properties of mixed Si-Ge nanocrystals of the form $Si_xGe_y:H_z$. All variables x, y and z have been varied within the symmetry restrictions and the current limitations imposed by our computing power. As before, we use the TDDFT/B3LYP high level *ab initio* method, the accuracy of which has been checked thoroughly, as we have seen many times up to now. It should be noted that up to date no such high level calculations exist for such systems. Limited ground-state zero-level calculations for $x+y=71$, using '*ab initio*' molecular dynamics have been published recently [38]. In addition a 'traditional' molecular dynamics and Monte-Carlo simulation for $x=y$ = 15, 30, 50, 256 and $z=0$ (without hydrogen) have appear lately [40], examining the segregation (only) of these species (no electronic or optical properties). The variation of the gap as a function of Ge (or Si) concentration is a multiple function, the points of which cannot be connected by a continues line because the same concentration can be realized in various ways. Instead of this diagram, we have plotted in Fig. 9 the variation of the optical gap for $x+y=71$ as a function of the diameter. For the sake of clarity we have chosen for this figure $x \approx y$ wherever possible. In the same figure the results for $x=0$, $y=71$ and $x=71$, $y=0$, for pure Ge and Si are displayed for comparison. As we can see in Fig. 9, even in this case the results for the optical gap, which as ex-

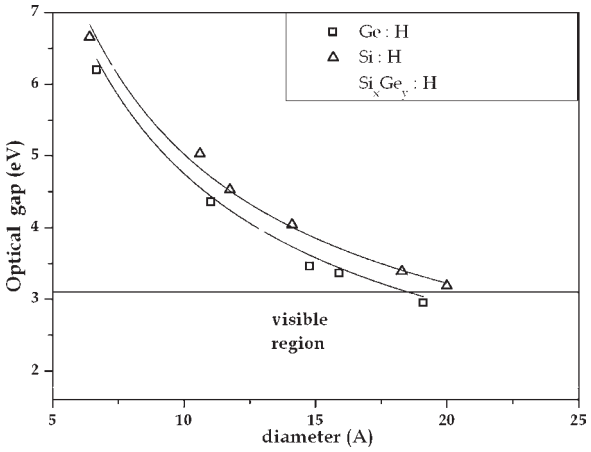

Fig. 9. Comparison of the optical gap variation of oxygen-free hydrogen-passivated silicon, germanium and silicon-germanium nanocrystals.

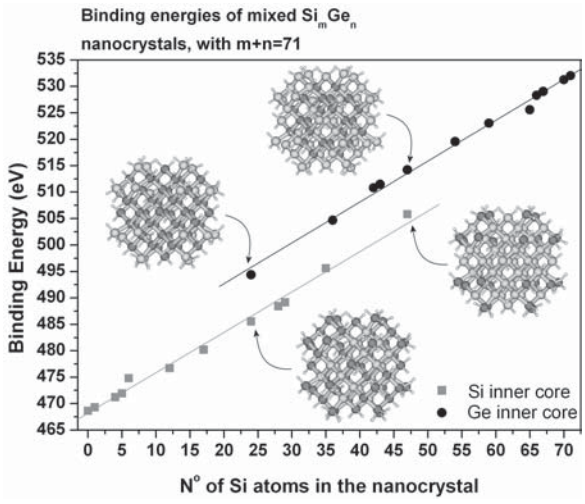

Fig. 10. Binding energy of mixed SinGem:H nanocrystals, with $n+m=71$, for varius substitutions of silicon atom layers by germanium layers. Representative nanocrystals are also shown in 'ball-and-stick' diagrams (Ge atoms are indicated by black spheres and Si atoms by grey spheres).

pected are lying between those of Si:H and Ge:H, cannot be connected by a continues line. The obvious reason is that the gap depends not only on the number of Ge atoms substituting layers of Si atoms, but also in the exact location of the layers. To investigate this dependence we have plotted in Fig. 10, the dependence of the binding energy (or 'atomization' energy) of the nanocrystals with $x+y=71$ as a function of y. As we can see, we have two distinct curves (parallel lines) depending on the exact location of the Ge layer relatively to the surface of the nanocrystals. It is clear from this plot that it is preferable to have the Ge atoms in the 'outer' part of the nanocrystal. Therefore, it is not surprising that the data of Fig. 9, for a constant total number of atoms, are not lying in one continuous line. The tendency of the Ge atoms to segregate onto the surface is energetically favoured due to the minimization of the energy cost of Ge versus Si bonds or of the dangling bonds in cases without hydrogen. The same conclusion was reached by Tarus *et al*. [40 48], for hydrogen-free SiGe nanoclusters Ge segregates onto the surface. The corresponding band (and optical) gaps for the nanocrystals with 'inner' Ge layers are higher compared to the 'outer' Ge layers. This is something that could be expected since, in general, the gaps of more stable species are usually higher. We can see therefore, in conclusion, that in the case of SiGe nanocrystals there new and more possibilities of band-gap adjustment and possible band-gap engineering.

6. RESULTS AND DISCUSSION FOR SILICON NANOCLUSTERS: THE SPECIAL CASE OF Si_6

6.1. Motivation (or the peculiar story of Si_6)

As mentioned earlier, small and medium size silicon clusters containing up to 100 atoms have been studied extensively both experimentally and theoretically due to their scientific and technological importance [41-46] However, even today several questions and puzzles still remain open here too, especially for bonding and structural properties, for which comparison between experimental and theoretical results is only indirect. This is especially true for large and moderate size clusters. For small clusters, such as Si_6, things have being considered much better. In particular Si_6 which is a magic cluster with increased stability is considered as one of the best and fully understood clusters [43-45]. Its structural and electronic properties have been studied theoretically (among others) by K. Ragavachari [42,44, 45], who is really the pioneer of the small cluster theoretical research. Ragavachari's final calculations [45], based in higher level methods (MP2 geometry optimization compared to his initial calculations with HF, see discussion at the end of section 2), were confirmed by experimental Raman measurements.

The confirmation was accomplished through the comparison and identification of the calculated and measured Raman-active vibration modes [45]. Thus, contrary to most of the other small Si clusters, Si_6 is considered as fully and well understood. Due to its 'magic' property, Si_6 is very popular and has been studied extensively both theoretically and experimentally. This is related to its small size, which makes the use of highest levels theoretical techniques possible, and its relative stability which facilitates its experimental characterization. Furthermore the characteristics of Si_6 have been used extensively to model and parameterize much larger systems through empirical and semi-empirical calculations. However, this is not the end of the story. More recent theoretical results [46], with much higher level theoretical techniques, for both energy gradients (geometry optimization, vibration frequencies) and energies, suggest different equilibrium structure for Si_6 than the one proposed (and 'verified') by Raghavachari and co-workers [45]. The irony of the story is that the new structure is similar to the structure Raghavachari has suggested earlier [44] by lower level methods. Not to mention also that Raghavachari himself have pioneered the development and implementation of some of the high-level techniques in popular computer packages. Thus, the story of Si_6 has 'suspense' and 'drama'! Yet it can serve at the same time as a best and worse case example of 'agreement' between (higher level) theory and experiment.

6.2. Questions and answers.

The initial structure proposed by Raghavachari on the basis of HF geometry optimization is the first structure on the left in Fig. 11, structure 11a [44]. This structure is an edge-capped trigonal bipyramid of C_{2V} symmetry. Following this structure there is a very close lying (in energy) bicapped tetrahedron, Fig. 11c, which can be also viewed as a face-capped trigonal bipyranmid of near C_{2V} symmetry. This last structure, initially of C_{2V} symmetry was unstable to distortions and was finally stabilized by further geometry optimization into the C_S (near C_{2V}) symmetric structure of Fig. 11c. The distorted octahedron of D_{4h} symmetry in Fig. 11b was unstable at the HF level of theory, so it was rejected as a local minimum of the energy 'hyper-surface'. When the geometry optimization is repeated at the MP2 level of theory, both of the low-lying structures, 11a and 11b, collapse into the same distorted octahedron structure of Fig. 11b. This lead Raghavachari to suggest that the real structure of Si_6 is the D_{4h} structure. On the experimental side, the measured Raman spectrum [45], seems to provide indirect support to the MP2 predictions, since the MP2 calculated spectrum for the D_{4h} structure, after a 5% scaling, appears to be in quite good agreement with experiment. Everything looks pretty natural up to here. Not quite!

In spite of this ideal agreement of (higher than before) theory and experiment, more recent results obtained with higher order perturbation as well as DFT/B3LYP theories by the present author [46] do not agree with the MP2 predictions. Instead, they agree with the general predictions of the HF gradients which favour the structure in Fig. 11a, but also the structure in Fig. 11c. The D_{4h} structure is not a local minimum for higher order perturbation theory as well as QCISD(T) and B3LYP [46]. This discrepancy is rather surprising since Si_6 is widely considered as a well-established system, almost a textbook case. Apparently, the perturbation expansion is not well converging and the energy hyper-surface is very flat. As a result of this flatness, the MP2 gradients fail to converge to the right structure. So what is it? Which structure of the three is the true

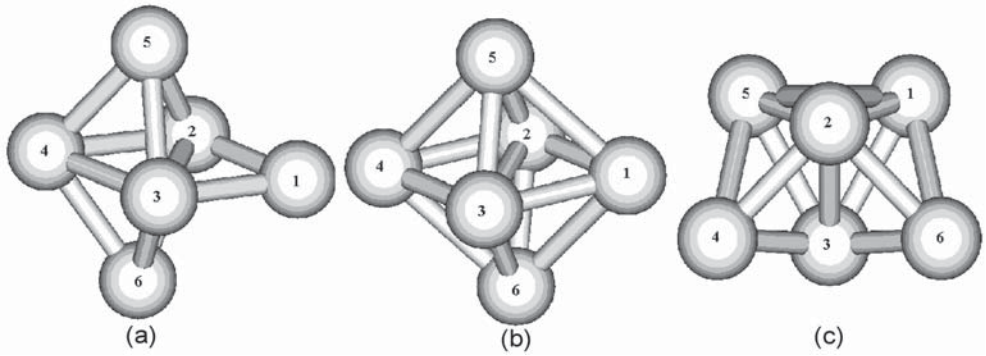

Fig. 11. The three (energetically) lowest-lying structures of the Si_6 cluster in a 'ball-and-stick' diagram.

structure of Si_6? The (paradoxical) answer is 'either all of them' or 'neither one'. To see why, let as have a closer look at Table 4 which includes the energies of all three structures in various higher-orders of theory from top to bottom, starting with MP2 and ending with the results of the QCISD(T) method. These calculations have been performed with a high quality basis set (so the technical approximations are at a relatively high level). As we can see, although the C_{2v} is the lowest possible structure, the energy differences between the three structures are marginal. The structures are practically and truly isoenergetic. The energy differences are smaller or comparable with the energy-accuracy of the calculations. What is even more important is that these differences are much smaller than the zero point energy of the nuclear vibrations or even smaller than the energies of the low frequency 'soft' modes. This is highly suggestive that the three structures could be continuously transforming between themselves at no energy cost through the soft vibrations. Are there any soft modes? Yes indeed. First of all, as we can see in table 6, at all levels of theory except MP2 the D_{4h} symmetric structure shows soft modes with imaginary frequencies. This indicates that this structure is not a global or local minimum but a saddle-point and that a lower symmetry structure can be more stable. Indeed, distorting the D_{4h} structure according to the displacement patterns of the imaginary frequency mode, shown in Fig. 12 (first from the left), we obtain under geometry optimization at higher levels of perturbation theory (e.g. MP3, MP4, etc) or B3LYP the edge-capped trigonal bipyramid of Fig. 11a. On the other hand soft modes (with no imaginary frequencies) have been also found in the other two structures. Thus, we have arrived to the same conclusion through a different route. The three structures could transform dynamically into each other through the coupling with soft (or unstable) vibration modes. We could recognize this effect as a dynamical Jahn-Teller effect, in analogy to the more familiar (static) Jahn-Teller effect, which is responsible for the (static) distortion of the high-symmetry ideal octahedron into the D_{4h} structure. The resulting structural non-rigidity of Si_6 is very unusual for such 'well-defined' system. There is an intriguing possibility that this structural non-rigidity of Si_6 could be related to its magic property. In this case the enhanced stability of the magic clusters would be a dynamic rather than a static property. This possibility is considered by the present author as highly probable [46]. Now everything seems to fit together nicely in principle, except for one thing. What about the experimental evidence (Raman frequencies) in favour of the D_{4h} structure? Let us have a closer look at Table 5. The last two columns of Table 4 show some selective frequency results for these structures, for modes compatible with D_{4h} Raman active modes and with large intensities. As we can see, these frequencies are comparable in magnitude to the experimental results and to the values predicted by MP3, MP4, B3LYP (and MP2) for the corresponding D_{4h} structure. However, both of these structures have a larger number of active modes (with much smaller intensities) than the ones shown in Table 4. Therefore, one possibility is that the experiment cannot detect all active Raman modes below some threshold value, or that it could not resolve frequencies which are 'nearby'. Independent of this, another alternative strong possibility is

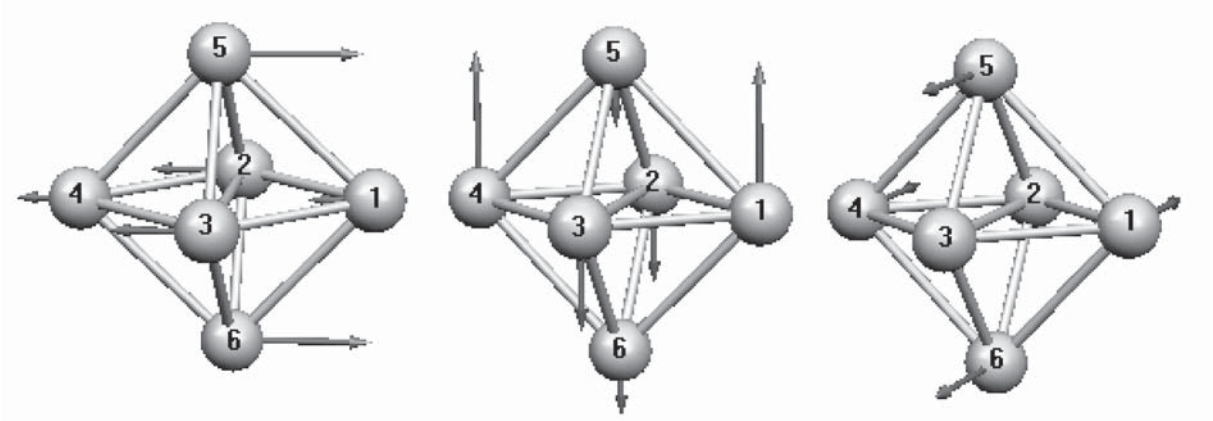

Fig. 12. The two unstable (first two from the left) and the first soft (on the right) modes of atomic vibrations for the distorted octahedron structure, in Fig. 11(b), of Si_6.

Table 4. Absolute energies for high-order methods in atomic units, together with relative energies in (eV) for QCISD(T), using the 'correlation consistent' cc-pVDZ basis set at the B3LYP/cc-pVDZ optimized geometry.

Method	Structures		
	C_S/C_{c2v}	C_{2V}	D_{4h}
MP2	-1734.0802651	-1734.0797177	-1734.0817634
MP4SDQ	-1734.0839215	-1734.0837717	-1734.0839383
MP4SDTQ	-1734.152869	-1734.1524312	-1734.1538008
QCISD	-1734.0786097	-1734.078665	-1734.0780716
QCISD(T)	-1734.1301978	-1734.1301368	-1734.1301309
	–	(+ 0.0017 eV)	(+0.0018 eV)
State	$^1A_1$	$^1A_1$	$^1A_{1g}$

that, since all three isomers coexist and transform into each other, experimental values reflect time-averages over the three structures. This last possibility is certainly more convincing after a closer look in the plots of Fig. 13, which show the calculated Raman spectrum of all three structures, together with the average of this spectrum and the experimentally measured Raman spectrum.

7. CONCLUDING REMARKS

The central issue of this review was the accurate theoretical description of the optical (primarily) and electronic properties of silicon-like and silicon-based semiconductor nanocrystals and nanoclusters. For obvious reasons of space and time limitations the discussion was focused on the optical and electronic properties of silicon, germanium and silicon-germanium nanocrystals, with particular emphasis on the role of surface oxygen and hydrogen in silicon nanocrystals. The possibility of band-gap engineering was given also special attention for Si-Ge nanocrystals, in view of the technological importance of these or similar systems (nanowires and nanoropes). The silicon nanoclusters were examined only through a particular example of the Si_6 cluster, which has a great scientific and technological, as well as epistemological and 'pedagogical' importance. In parallel to the main focus, as a secondary byproduct of this review, the present author has tried

Table 5. Vibrations of the Si6 D4h structure at various levels of theoretical treatment. Some 'corresponding' frequencies are also given for the C2V and CS structures. Frequencies are given in cm^{-1}. The symbol i indicates imaginary frequencies

D_{4h} Exp. Freq. Ref. [45]	D_{4h} Sym	MP2 5% scaled Ref. [45]	MP2	MP3	MP4	B3LYP	C_{2v} B3LYP	C_s B3LYP
–	E_u	–	52	8li	75i	79i	–	–
–	B_{2u}	–	197	117	149	117	–	–
252	B_{2g}	209	220	252	225	234	276	276
300	A_{1g}	298	314	331	319	312	295	295
–	A_{2u}	–	358	344	347	315	–	–
386	B_{1g}	376	396	418	404	386	361	360
404	E_g	425	447	424	421	395	395	370
458	A_{1g}	457	481	480	476	442	436	439
							460	448
								451
–	E_u	–	482	483	480	443		

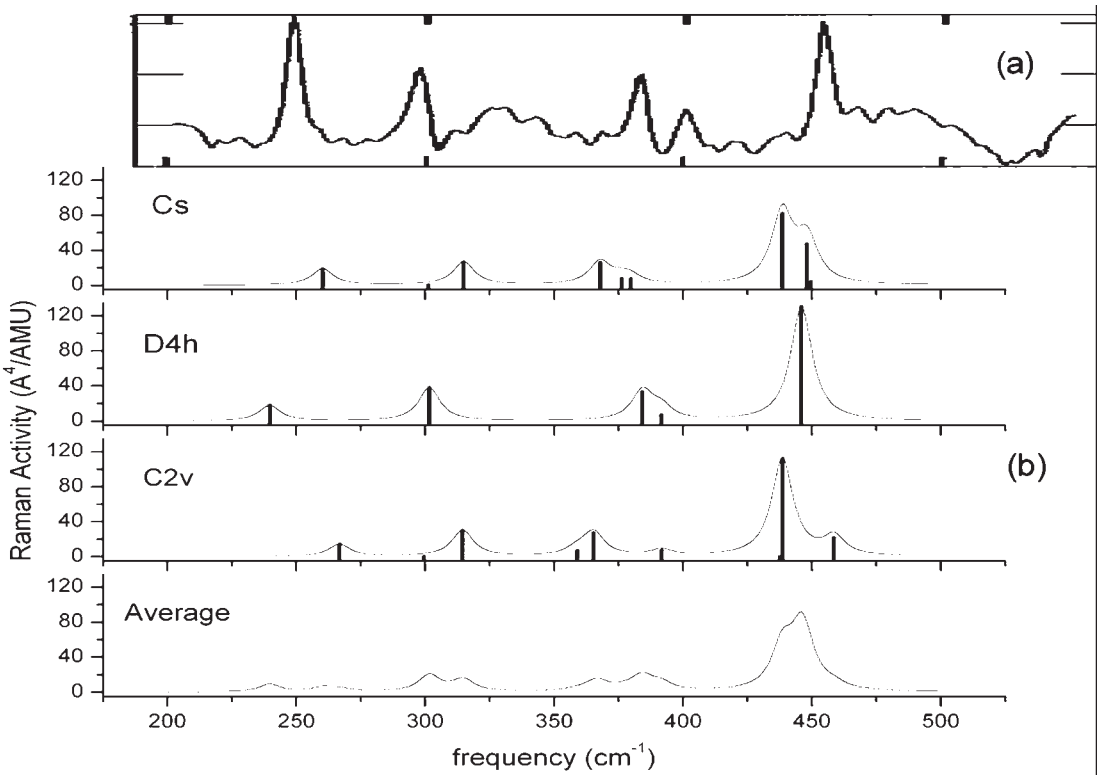

Fig. 13. The measured (a) and calculated (b) Raman spectrum for the three lowest isoenergetic structures of the Si_6 cluster.

to bring up some 'epistemological' and 'real-life' components of scientific research, such as the struggle of a scientist (theorist or experimentalists) to face the challenges and try to fit all pieces of the puzzles together. This is not always easy. Contradictions, paradoxes and controversial issues always take long time (sometimes infinite) to be settled but this is one of the most beautiful aspects of scientific research. As we have seen, at the end the various pieces of the early (and later) puzzles seem to fit together nicely in a consistent way (or maybe not?). It must not be forgotten however, that theoretical results, no matter how accurate, are models of the real systems idealized in one way or another. It is not always possible in the complex preparation and characterization conditions prevailing during most of the experiments to make one-to-one correspondence with the theoretical models, unless the experiments have been performed in a well defined and well characterized way with clear and reliable error bars. This is not always easy; and it is even more difficult to decide which of the existing experiments satisfy these criteria. The accurate theoretical results (even for idealized systems) can then serve as a 'yardstick' in order to 'calibrate' and decide on the measurements. At the same time, although theoretical results deal with well-defined model systems, their accuracy is not always easy to access since it depends not only on the level and the accuracy of the underlying theory, but it is also characterized by all secondary theoretical and technical approximations, as well as by the experimental input they take into account. Nevertheless it is much easier to pinpoint the weak points of theoretical results, compared to those of experiments (this is only a personal view). In any case, results (theoretical or experimental) are not always what they claim (or appear) to be, unless proven otherwise. This is certainly true for the results presented here.

ACKNOWLEDGEMENTS

The research work on silicon nanocrystals was performed in collaboration with C. S. Garoufalis. The research work on Ge and SiGe nanocrystals was performed in collaboration with C. S. Garoufalis, M. S. Skaperda, and E. N. Koukaras. Most of the drawings and the art work on Si_6 cluster was taken care of by Mr. E. N. Koukaras. We thank the European

Social Fund (ESF), Operational Program for Educational and Vocational Training II (EPEAEK II), and particularly the Program PYTHAGORAS, for funding the above work.

REFERENCES

[1] L. T. Canham // *Appl. Phys. Lett.* **57** (1990) 1046.
[2] J.P. Wilcoxon, G. A. Samara and P. N. Provencio // *Phys. Rev. B* **60** (1999) 2704.
[3] M. V. Wolkin, J. Jorne and P. M. Fauchet, G. Allan and C. Delerue // *Phys. Rev. Lett.* **82** (1999) 197.
[4] F. A.Reboredo A. Franceschetti and A. Zunger // *Phys. Rev. B* **61** (2000) 13073.
[5] Schuppler, S.L. Friedman, M.A. Marcus, D.L. Adler, Y.H. Xie, F.M. Ross, Y.L. Cha-bal, T.D. Harris, L.E. Brus, W.L. Brown, E.E. Chaban, P.F. Szajowski S.B. Christman and P.H. Citrin // *Phys Rev. Lett.* **72** (1994) 2648; *Phys. Rev. B* **52** (1995) 4910.
[6] A. Franceschetti and A. Zunger // *Phys. Rev. Lett.* **78** (1997) 915.
[7] C. S. Garoufalis, A. D. Zdetsis and S. Grimme // *Phys. Rev. Lett.* **87** (2001) 276402.
[8] M. Rohlfing and S.G.Louie Phys // *Rev. Lett.* **80** (1998) 3320.
[9] S. Ogut, J. Chelikowsky and S. G. Louie // *Phys. Rev. Lett.* **79** (1997) 1770; *Phys. Rev. Lett.* **80** (1998) 3162.
[10] J. L. Gole and D. A. Dixon // *Phys. Rev. B* **57** (1998) 12002.
[11] L.E. Brus, P.F. Szajowski, W.L. Wilson, T. D. Harris, S. Schuppler, and P.H. Citrin // *J. Am. Chem. Soc.* **117** (1995) 2915.
[12] K. Kim // *Phys. Rev B* **57** (1998) 13072.
[13] S. Furukawa and T. Miyasato // *Phys. Rev. B* **38** (1988) 5726.
[14] Y. Kanemitsou // *Phys.Rev. B* **49** (1994) 16845.
[15] J. Muscat, A. Wander and N.M. Harrison // *Chem. Phys. Lett.* **342** (2001) 397.
[16] I. Vasiliev, S. Ogut and J. Chelikowsky // *Phys. Rev. Lett.* **86** (2001) 1813.
[17] A. Puzder, A.J. Williamson, J. C. Grossman and G. Galli // *Phys. Rev. Lett.* **88** (2002) 097401.
[18] I. Vasiliev, J. R. Chelikowsky and R. M. Martin // *Phys. Rev. B* **65** (2002) 121302-1.
[19] E. Degoli, G. Cantele, E. Luppi, R. Magri, D. Ninno, O. Bisi and S. Ossicini // *Phys. Rev. B* **69** (2004) 155411.
[20] H. Weissker, J. Furthmuller and F. Bechstedt // *Phys. Rev. B* **67** (2003) 245304.
[21] A. Franceschetti and S. T. Pantelides // *Phys. Rev. B* **68** (2003) 033313.
[22] A. Puzder, A. J. Williamson, J. C. Grossman and G. Galli // *J. Am. Chem. Soc.* **125** (2003) 2786.
[23] A. J. W Williamson, J. C. Grossman, R. Q. Hood, A. Puzder and G. Galli // *Phys. Rev. Lett.* **89** (2002) 196803; A. Puzder, A. J. Williamson, J. C. Grossman and G. Galli // *J. Chem. Phys.* **117** (2002) 6721.
[24] O. Akcakir, J. Therrien, G. Belomoin, N. Barry, J. D. Muller, E. Gratton and M. Nayfeh // *App. Phys. Lett.* **76** (2000) 1857.
[25] L. Mitas, J. Therrien, R. Twesten, G. Belomoin and M. Nayfeh // *App. Phys. Lett.* **78** (2001) 1918.
[26] S. Rao, J. Sutin, R. Clegg, E. Gratton, M. H. Nayfeh, S. Habbal, A. Tsolakidis and R. Martin // *Phys. Rev B* **69** (2004) 205319-1.
[27] Zhiyong Zhou, Louis Brus and Richard Friesner // *NanoLetters* **3** (2003) 163.
[28] M. Luppi and S. Ossicini // *J. App. Phys.* **94** (2003) 2130.
[29] Zhiyong Zhou, Richard A. Friesner and Louis Brus // *J.Am. Chem Soc.* **125** (2003) 15599.
[30] A.D. Zdetsis, C. S. Garoufalis and Stefan Grimme, In: *NATO Advanced Research Workshop on "Quantum Dots: Fundamentals, Applications, and Frontiers"* (Crete 2003), ed. by B.A. Joyce *et al.* (Kluwer-Springer, 2005) p. 317.
[31] C.S. Garoufalis and A. D. Zdetsis // *J. Physics conference series* (2005) in press); C.S. Garoufalis and A. D. Zdetsis, submitted
[32] J. P. Wilcoxon, P. P. Provencio and G. A. Samara // *Phys. Rev. B* **64** (2001) 035417.
[33] J. R. Heath, J. J. Shiang and A. P. Alivisatos // *J. Chem. Phys.* **101** (1994) 1607.
[34] O. G. Palummo and R. Del Sole // *Phys. Stat. sol.* **175** (1999) 23.
[35] H. Weissker, J. Furthmüller and F. Bechstedt // *Phys. Rev. B* **65** (2002) 155328.
[36] D. V. Melnikov and J.R. Chelikowsky // *Solid State Commun.* **127** (2003) 361.
[37] A. D. Zdetsis, C.S. Garoufalis and M. S. Skaperda // *J. Physics conference series* (2005) in press; A. D. Zdetsis and C.S. Garoufalis, submitted.

[38] M. Yu, C. S. Jayanthi, D. A. Drabold and S. Y. Wu // *Phys. Rev. B* **68** (2003) 035404.
[39] A. D. Zdetsis, C.S. Garoufalis, M. S. Skaperda and E. N. Koukaras // *J. Physics conference series* (2005), in press; A. D. Zdetsis and C.S. Garoufalis, submitted.
[40] J. Tarus, M. Tantarimaki and K. Nordlund // *Nucl. Instr. Meth. B* **228** (2005) 51.
[41] R. P. Andres *et al.* // *J. Mat. Res.* **4** (1989) 704.
[42] K. Raghavachari // *Phase Transitions* **24-26** (1990) 61.
[43] M. F. Jarrold // *Science* **252** (1991) 1085.
[44] K. Raghavachari // *J. Chem. Phys.* **84** (1986) 5672.
[45] E. C. Honea *et al.* // *Nature* **366** (1993) 42; E. C. Honea *et al.* // *J. Chem. Phys.* **110** (1999) 12161.
[46] A. D. Zdetsis // *Phys. Rev. A* **64** (2000) 023202; A.D. Zdetsis, to be published.
[47] M.E.Casida, In: *Recent Advances in density functional methods*, Vol. 1, ed. by D.P.Chong (World Scientific, Singapore, 1995).
[48] P. J. Stephens, F. J. Devlin, C. F. Chabalowski and M. J. Frisch // *J. Phys. Chem* **98** (1994) 11623.
[49] A. D. Becke // *Phys.Rev.A* **38** (1988) 3098; J. P. Perdew // *Phys.Rev. B* **33** (1986) 8822.
[50] G. Rajagopal *et al.* // *Phys. Rev. Lett.* **73** (1994) 1959; G. Rajagopal *et al*. // *Phys. Rev. B* **51** (1995) 10591.
[51] *TURBOMOLE* (Vers. 5.3),Universitat Karlsruhe, 2000.
[52] A. Schafer, H. Horn and R. Ahlrichs // *J.Chem. Phys*. **97** (1992) 2571.
[53] R. Bauernschmitt and R. Ahlrichs // *Chem. Phys. Lett.* **256** (1996) 454.
[54] S. Grimme and M. Waletzke *Phys.Chem.Chem.Phys.* **2** (2000) 2075.